IEEE Access
Multidisciplinary | Rapid Review | Open Access Journal

Received December 3, 2020, accepted December 24, 2020, date of publication December 29, 2020, date of current version January 7, 2021.

Digital Object Identifier 10.1109/ACCESS.2020.3047742

Analytical Sub-Domain Model for Magnetic Field Computation in Segmented Permanent Magnet Switched Flux Consequent Pole Machine

WASIQ ULLAH[1], FAISAL KHAN[1], (Member, IEEE), ERWAN SULAIMAN[2], IRFAN SAMI[3], AND JONG-SUK RO[3]

[1]Department of Electrical and Computer Engineering, COMSATS University Islamabad, Abbottabad Campus, Abbottabad 22060, Pakistan
[2]Department of Electrical Power Engineering, Universiti Tun Hussein Onn Malaysia, Parit Raja 86400, Malaysia
[3]School of Electrical and Electronics Engineering, Chung-Ang University, Seoul 06974, South Korea

Corresponding author: Jong-Suk Ro (jongsukro@gmail.com)

This work was supported by the Human Resources Development (No. 20204030200090) of the Korea Institute of Energy Technology Evaluation and Planning (KETEP) grant funded by the Korea government Ministry of Trade, Industry, and Energy. This research was also supported by the Korea Research Fellowship Program through the National Research Foundation (NRF) of Korea funded by the Ministry of Science and ICT (2019H1D3A1A01102988).

ABSTRACT Computational complexity, magnetic saturation, complex stator structure and time consumption due to repeated iteration compels researchers to adopt alternate analytical model for initial design of electric machines especially Switched Flux Machine (SFM). To overcomes the abovesaid demerits, In this article alternate analytical sub-domain model (SDM) for magnetic field computation in Segmented PM switched flux consequent pole machine (SPMSFCPM) with flux bridge and flux barriers accounting boundary and interface conditions, radial magnetized PMs (RM-PMs) and circumferential magnetized PMs (CM-PMs), interaction between stator slots and inner/outer rotor topologies is proposed. Overall field domain is divided into air gap, stator slots and Permanent Magnet (PM) accounting influence of CM/RM-PMs under no-load and on-load conditions. Analytical expression of field domain is obtained by solving magnetic vector potential utilizing Maxwell's equations. Based on the magnetic field computation especially no-load and on-load condition, Magnetic Flux Density (MFD) components, open-circuit flux linkage, mechanical torque and cogging torque are computed utilizing Maxwell Stress Tensor (MST) method. Moreover, developed analytical SDM is validated with globally accepted Finite Element Analysis (FEA) utilizing JMAG Commercial FEA Package v. 18.1 which shows good agreement with accuracy of ∼98%. Hence, authors are confident to propose analytical SDM for initial design of SPMSFCPM to suppress computation time and complexity and eliminate requirements of expensive hardware and software tools.

INDEX TERMS AC machines, consequent pole, flux barrier, sub-domain model, permanent magnet, switched flux machine, Maxwell equations, Maxwell stress tensor.

I. INTRODUCTION

Flux switching Machines (FSMs) are classified in to three classes based on excitation source i.e. Permanent Magnet (PM) excitation, Field winding excitation and Hybrid excitation [1]. Among the aforesaid FSMs classes, due to high torque and power density, PM excited machines are widespread in domestic and industrial applications [2]. Due to double salient nature and robust rotor, FSMs are considered as appropriate applicants for high speed brushless AC application. Various topology of PM excited FSMs are reported in literature (as shown in Figure. 1) when high torque and power density are primitive prerequisite, however existing topology are associated with excessive rare earth PM usage, leakage flux and flux circulation. To overcome aforesaid demerits, this article introduces Segmented PM Switched Flux Consequent Pole Machine (SPMSFCPM) as shown in Figure. 2. Structure of proposed SPMSFCPM is composed passive rotor (made of iron) and stator core encompassing of armature windings slots and Segmented PMs configuration enclosing Radial Magnetized PMs (RM-PMs) and Circumferential Magnetized PMs (CM-PMs) with in flux bridges and flux barriers.

All classes of FSMs and proposed SPMSFCPM are accurately modelled employing numerical based Finite Element Analysis (FEA) tools however despite of expensive

The associate editor coordinating the review of this manuscript and approving it for publication was Giambattista Gruosso.

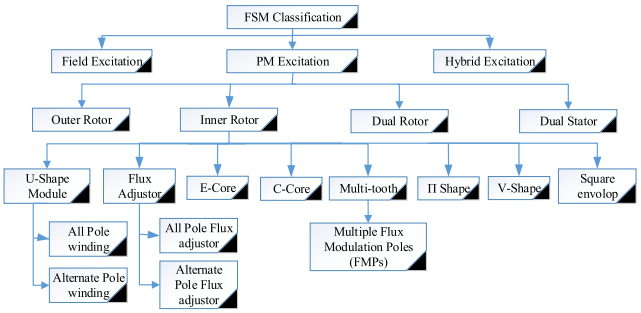

FIGURE 1. FSM classes and topologies classification.

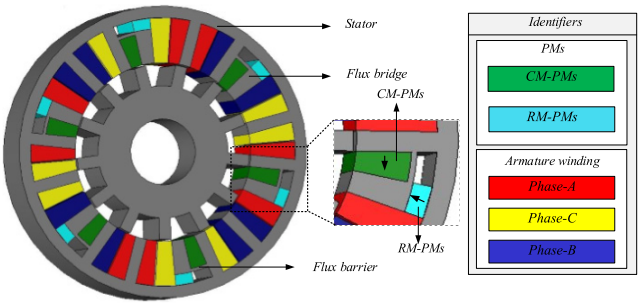

FIGURE 2. Proposed SPMSFCPM 3D cross sectional view.

hardware/software, large drive storage, repeated iterative process, complex stator design and PM non-linear behaviour increases computational time and computational complexity. To overcome the aforesaid demerits, analytical modelling is preferred for initial design purpose [3]. Analytical techniques accurately predict magnetic field distribution in shorter time [4]–[6]. A comprehensive review on analytical modelling approaches is illustrated in [7], [8] and discussed for automate numerically mapping, Schwarz–Christoffel (SC) method is developed utilizing SC MATLAB toolbox. This mapping offers efficient analysis tool and allows polygonal boundaries transformation to simpler domain. SC method ease in problems come across in solving complicated boundary value problems [9]. However, this technique suffers from difficulties and complexity related to evaluation of mapping function.

Boundary Element Method (BEM) is formulated based on Poisson and Laplace equations in integral form for magnetic field computation. In BEM, boundary domain is evaluated based on integral equation which helps in significant element number compared with corresponding FEA [10]. However, BEM have limited application due to linear material property in devices with soft-magnetic material i.e. electric machines [11].

Fourier Modelling (FM) is particularly interesting in periodic structure, however FM doesn't account magnetic permeability [12] which is momentous downside in stator/rotor slotting [13]. Author in [14]–[16] investigates hybrid analytical modelling (HAM) based on FM and meshed magnetic equivalent circuit (MEC). HAM consider small geometric structures and material permeability. Mesh-based MEC linked to one side of FM is evaluated in [15]–[18]. Magnetic field computation in air-gap with promising results is discussed in [15] whereas electromagnetic performance i.e. cogging torque is precisely estimated in [16]. However, origin of MEC construction about saturation is not explained.

Saturated structure machines are being investigated by Magnetic Equivalent Circuits (MEC) modelling to predict open circuit phase linkage [19]. This modelling technique is dependent on flux paths and tubes in airgap [20], [21]. It uses permeance and reluctance for determination of performance parameters, but it only deals with airgap and neglects the effect of rotor, stator and machine geometry. However, abovesaid deficiencies are catered using Lumped Parameter Magnetic Equivalent Circuit (LPMEC) [22], [23].

In this article, a comprehensive overview of the analytical sub-domain model accounting boundary and interface conditions, influence of RM-PMs and CM-PMs, interaction between stator slots and inner/outer rotor topologies are presented and compared with FEA for design of SPMSFCPM. Overall article is order as, section II illustrates SPMSFCPM design methodology, section III present analytical sub-domain modelling. Section IV shows computation of electromagnetic performance, section V analyzed validations of analytical sub-domain modelling for initial design of SPMSFCPM and lastly important conclusions are discussed in section VI.

II. SPMSFCPM DESIGN METHODOLOGY

Design variables of SPMSFCPM are specified in Figure. 3 and listed in Table 1. Design of SPMSFCPM model as shown in Figure. 2 shows that SPMSFCPM stator core is comprised of E-core stator slot structure with alternate h-shaped stator tooth which enclosed CM-PMs and RM-PMs to diminish stator leakage flux. RM-PMs helps in leakage flux suppression from PMs poles resulting an improved magnetic flux density in the stator yoke and hence improving the flux linkage by

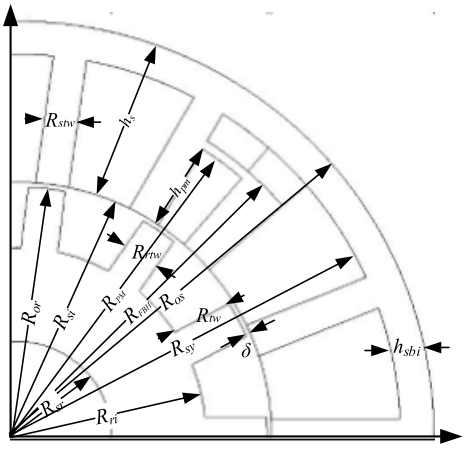

FIGURE 3. Design variables of SPMSFCP.

TABLE 1. Design parameters of CPSFPMM.

Parameter	Symbol	Dimension
Outer radius of stator, (mm)	R_{os}	45
Inner radius of stator yoke, (mm)	R_{sy}	41.4
Outer radius of PM, (mm)	R_{PM}	37
Stator back iron height, (mm)	h_{sbi}	3.6
Inner radius of stator, (mm)	R_{si}	27.5
Inner radius of rotor, (mm)	R_{ri}	20.4
Outer radius of rotor, (mm)	R_{or}	27
Rotor tooth width, (mm)	R_{rtw}	4
Stator slot width, (mm)	R_{stw}	4
CM-PM height, (mm)	h_{pm}	8.5
Rotor shaft radius, (mm)	R_{sr}	10.2
Radius of flux bridge, (mm)	R_{FBH}	36
Air gap length, (mm)	δ	0.5
Stator height, (mm)	h_s	17.5
Stack length, (mm)	L	25
Relative Permeability of PMs	μ_r	1.05
Current density, (A/mm^2)	J	15
Remanence of PMs, (T)	B_r	1.2

passing through alternative flux bridges and flux barriers and link to the rotor.

Proposed SPMSFCPM improve magnetic field distribution. The flux linkage in proposed design occur through stator yoke as well as flux bridge with negligible reluctance. Thus, magnetic field distribution and flux linkage between rotor and stator in SPMSFCPM is stronger compared to the conventional state of the art. Magnetic flux density mapping of SPMSFCPM is shown in Figure. 4.

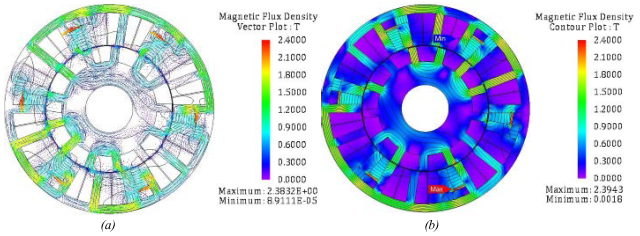

FIGURE 4. Nephogram of magnetic flux density (a) vector plot (b) Contour plot.

III. ANALYTICAL SUB-DOMAIN MODELLING

Two steps analysis elaborate overall Sub-Domain modelling (SDM). In 1st step the overall machine field domains are classified into regions i.e. Region I: air-gap, Region II: CM/RM-PMs and Region III: stator slots as shown in Figure 5 whereas in 2nd step, boundary and interface condition are employed on specified field regions. In SDM, expression for aforesaid field domains are formulated in the form of Fourier expressions accounting boundary and interface conditions. Based on Fourier expressions, relationship between Fourier coefficient and source (CM/RM-PMs and armature current) is formed in the form of first order multivariable utilizing boundary and interface conditions.

A. GENERAL VECTOR POTENTIAL

Poisson function accounting influence of source (PMs and armature current density) in the field domains are utilized for general vector potential (GVP) solution which is expressed as

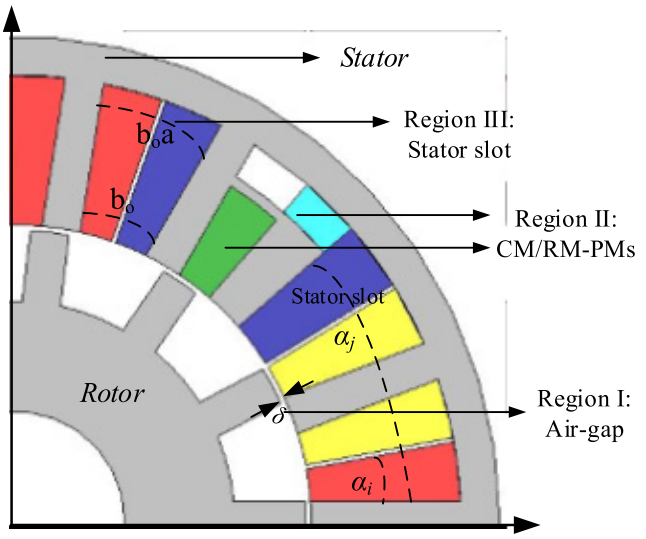

FIGURE 5. Division of filed domains in SDM.

$$\frac{\partial^2 A_z}{\partial r^2}+\frac{1}{r}\frac{\partial A_z}{\partial r}+\frac{1}{r^2}\frac{\partial^2 A_z}{\partial \alpha^2}=\begin{cases}\left(\dfrac{\partial M_r}{\partial \alpha}-M_\alpha\right)\mu_o/r, & \text{in PMs}\\ 0, & \text{in air-gap}(\delta)\\ -J\mu_o, & \text{in Statorslot}\end{cases} \tag{1}$$

GVP solution for three field domains i.e. δ, CM/RM-PMs and stator slots are expressed as

$$A_{zI}=\left[\sum_k\left(A_{Ik}\left(\frac{r}{R_{ri}}\right)^k+B_{Ik}\left(\frac{r}{R_{ri}}\right)^{-k}+\frac{M_{ck\gamma}}{\mu_r\left(1-k^2\right)}\right)\cos(\alpha k)+\sum_k\left(C_{Ik}\left(\frac{r}{R_{ri}}\right)^k+D_{Ik}\left(\frac{r}{R_{ri}}\right)^{-k}\frac{M_{sk\gamma}}{\mu_r\left(1-k^2\right)}\right)\sin(\alpha k)\right] \tag{2}$$

$$A_{zII}=\left[\sum_k\left(A_{IIk}\left(\frac{r}{R_{si}}\right)^k+B_{IIk}\left(\frac{r}{R_{ri}}\right)^{-k}\right)\cos(\alpha k)+\sum_k\left(C_{IIk}\left(\frac{r}{R_{si}}\right)^k+D_{IIk}\left(\frac{r}{R_{ri}}\right)^{-k}\right)\sin(\alpha k)\right] \tag{3}$$

$$A_{zIII}=\mu_o J_{io}\left(R_{sy}^2\ln\left(r-r^2\right)\right)/2+\left[\sum_k\left(\frac{J_{in}\mu_o}{F_n^2-4}r^2\right)\cos\left[\frac{\pi n}{d_{sa}}\left(\alpha-\alpha_i+0.5d_{sa}\right)\right]+\sum_k\left(C_iR_{si}/R_{sy}\left(\frac{r}{R_{sy}}\right)^{\frac{\pi n}{d_{sa}}}+C_i\left(\frac{r}{R_{si}}\right)^{-\frac{\pi n}{d_{sa}}}\right)\cos\left[\frac{\pi n}{d_{sa}}\left(\alpha-\alpha_i+0.5d_{sa}\right)\right]\right] \tag{4}$$

where k is harmonics order, A_{Ik}, B_{Ik}, C_{Ik}, D_{Ik}, A_{IIk}, B_{IIk}, C_{IIk}, and D_{IIk} are Fourier coefficient of the sub-regions such as air-gap and PMs respectively which are computed utilizing boundary and interface conditions.

B. SOURCE

Segmented PMs (CM/RM-PMs) and armature current density is major excitation source in SPMSFCPM. Magnetization Patterns (MP) of PMs are represented as sum of sine and cosine harmonics terms utilizing magnetization distribution function [24], [8].

$$M = M_r r + M_\theta \alpha \tag{5}$$
$$M_r = \sum_{k=1,3\ldots} M_{rk} \cos(\alpha k - \omega_r k t - \alpha_o k) \tag{6}$$
$$M_r = \sum_{k=1,3\ldots} (M_{rck} \cos(\alpha k) + M_{rsk} \sin(\alpha k)) \tag{7}$$
$$M_\theta = \sum_{k=1,3} M_{\theta k} \sin(\alpha k - \omega_r k t - \alpha_o k) \tag{8}$$
$$M_\theta = \sum_{k=1,3\ldots} (M_{\theta ck} \cos(\alpha k) + M_{\alpha sk} \sin(\alpha k)) \tag{9}$$

whereas M_r is radial magnetization component and M_θ are tangential magnetization component.

$$M_{rck} = M_{rk} \cos(\omega_r k t + \alpha_o k) \tag{10}$$
$$M_{rsk} = M_{rk} \sin(\omega_r k t + \alpha_o k) \tag{11}$$
$$M_{\theta ck} = -M_{\theta k} \sin(\omega_r k t + \alpha_o k) \tag{12}$$
$$M_{\theta sk} = M_{\theta k} \cos(\omega_r k t + \alpha_o k) \tag{13}$$

whereas ω_r is rotational speed, M_{rsk} and $M_{\theta sk}$ is amplitude of k_{th} order sine radial and tangential MP, M_{rck} and $M_{\theta ck}$ is amplitude of k_{th} cosine radial and tangential MP.

$$M_k = M_{rk} + k M_{\theta k} \tag{14}$$
$$M_{ck} = M_k \cos(\omega_r k t + \alpha_o k) = M_{rck} + k M_{\theta sk} \tag{15}$$
$$M_{sk} = M_k \sin(\omega_r k t + \alpha_o k) = M_{rsk} - k M_{\theta sk} \tag{16}$$

MP for M_{rk} and $M_{\theta k}$ varies i.e.
For RM-PMs

$$M_{rk} = \frac{4 B_r P}{\pi k \mu_o} \sin\left(\frac{0.5\pi\alpha_p k}{P}\right) \quad for\ k/p = 1, 3, 5\ldots \tag{17}$$
$$M_{rk} = \frac{4 B_r}{\pi \mu_o k/p} \sin\left(0.5\pi\alpha_p \left(\frac{k}{p}\right)\right) \quad for\ k/p = 1, 3, 5\ldots \tag{18}$$

For CM-PMs

$$M_{rk} = \frac{B_r}{\mu_o}\alpha_p \left(\frac{\sin\left[(k+1)\,\alpha_p\left(\frac{\pi}{2P}\right)\right]}{(k+1)\,\alpha_p\left(\frac{\pi}{2P}\right)} + \frac{\sin\left[(k-1)\alpha_p(\pi/2P)\right]}{(k-1)\alpha_p(\pi/2P)}\right) \tag{19}$$
$$M_{\theta k} = \frac{B_r}{\mu_o}\alpha_p \left(\frac{\sin\left[(k+1)\alpha_p(\pi/2P)\right]}{(k+1)\alpha_p(\pi/2P)} - \frac{\sin\left[(k-1)\alpha_p(\pi/2P)\right]}{(k-1)\alpha_p(\pi/2P)}\right) \tag{20}$$

where $\alpha_p = pole\ arc/pole\ pitch$.

For non-overlap winding pattern in stator slot, Current density (J) in the i_{th} armature winding slots can be expressed as [25]

$$J = (J_{i1} + J_{i2})/2 + \sum J_{in} \cos\left[\frac{n\pi}{d_{sa}}(\alpha - \alpha_i + d_{sa}/2)\right] \tag{21}$$
$$J = 2/\pi n\,(J_{i1} - J_{i2}) \sin(\pi n/2) \tag{22}$$

C. MAGNETIC FLUX DENSITY

Magnetic flux density (MFD) is associated with Radial (B_r) and tangential (B_θ) components which are expressed as

$$B_r = \left(\frac{1}{r}\right)\frac{\partial A_z}{\partial \alpha} \tag{23}$$
$$B_\theta = -\frac{\partial A_z}{\partial r} \tag{24}$$

B_r and B_θ in term of Fourier coefficients i.e. A_{Ik}, B_{Ik}, C_{Ik} and D_{Ik} for airgap, A_{IIk}, B_{IIk}, C_{IIk} and D_{IIk} for CM/RM-PMs and stator slots are expressed as

$$B_{Ir} = \frac{1}{r}\sum_k -k\left[A_{Ik}\left(\frac{r}{R_{si}}\right)^k + B_{Ik}\left(\frac{r}{R_{ri}}\right)^{-k}\right]\sin(k\alpha) + \frac{1}{r}\sum_k k\left[C_{Ik}\left(\frac{r}{R_{si}}\right)^k + D_{Ik}\left(\frac{r}{R_{ri}}\right)^{-k}\right]\cos(k\alpha) \tag{25}$$

$$B_{I\theta} = -\sum_k -k\left[\frac{A_{Ik}}{R_s}\left(\frac{r}{R_{si}}\right)^{k-1} + \frac{B_{Ik}}{R_{ri}}\left(\frac{r}{R_{ri}}\right)^{-k-1}\right]\cos(k\alpha) - \sum_k k\left[\frac{C_{Ik}}{R_{si}}\left(\frac{r}{R_{si}}\right)^{k-1} + \frac{D_{Ik}}{R_{ri}}\left(\frac{r}{R_{ri}}\right)^{-k-1}\right]\sin(k\alpha) \tag{26}$$

$$B_{IIr} = \frac{1}{r}\sum_k -k\left[A_{IIk}\left(\frac{r}{R_{ri}}\right)^k + B_{IIk}\left(\frac{r}{R_{ri}}\right)^{-k} + \frac{\mu_o M_{ck} r}{(k^2-1)}\right]\sin(k\alpha) + \frac{1}{r}\sum_k k\left[C_{IIk}\left(\frac{r}{R_{ri}}\right)^k + D_{IIk}\left(\frac{r}{R_{ri}}\right)^{-k} + \frac{\mu_o M_{sk} r}{(k^2-1)}\right]cos(k\alpha) \tag{27}$$

$$B_{II\theta} = \sum_k \left[\frac{A_{IIk}}{R_{si}}\left(\frac{r}{R_{ri}}\right)^{k-1} - \frac{B_{IIk}}{R_{ri}}\left(\frac{r}{R_{ri}}\right)^{-k-1} + \frac{\mu_o M_{ck}}{(k^2-1)}\right]\cos(k\alpha) + \sum_k \left[\frac{C_{IIk}}{R_{ri}}\left(\frac{r}{R_{ri}}\right)^{k-1} - \frac{D_{IIk}}{R_{ri}}\left(\frac{r}{R_{ri}}\right)^{-k-1} + \frac{\mu_o M_{sk}}{(k^2-1)}\right]\sin(k\alpha) \tag{28}$$

$$B_{IIIr} = -\sum_k \left\{ \left[\frac{n\pi}{d_{sa}} C_i \left(\left(\frac{R_{si}}{R_{sy}} \right)^{\frac{n\pi}{d_{sa}}} + \left(\frac{r}{R_{si}} \right)^{-\frac{n\pi}{d_{sa}}} \right) \right] / r + J_{in}\mu_o \left[\frac{n\pi}{d_{sa}} r - 2R_{sy} \left(\frac{r}{R_{sy}} \right)^{\frac{n\pi}{d_{sa}}-1} \right] \Big/ \left(\left(\frac{n\pi}{d_{sa}} \right)^2 - 4 \right) \right\} \times \sin \left[\frac{n\pi}{d_{sa}} (\alpha - \alpha_i + 0.5 d_{sa}) \right] \quad (29)$$

$$B_{III\theta} = -0.5 J_{io}\mu_o \left(R_{sy}^2 - r^2 \right) / r - \sum_k \left\{ \left[\frac{n\pi}{d_{sa}} C_i \left(\left(\frac{R_{si}}{R_{sy}} \right)^{\frac{n\pi}{d_{sa}}} - \left(\frac{r}{R_{si}} \right)^{-\frac{n\pi}{d_{sa}}} \right) \right] / r + 2 J_{in}\mu_o \left[r - 2R_{sy} \left(\frac{r}{R_{sy}} \right)^{\frac{n\pi}{d_{sa}}-1} \right] \Big/ \left(\left(\frac{n\pi}{d_{sa}} \right)^2 - 4 \right) \right\} \times \cos \left[\frac{n\pi}{d_{sa}} (\alpha - \alpha_i + 0.5 d_{sa}) \right] \quad (30)$$

D. BOUNDARY AND INTERFACE CONDITION

The aforesaid Fourier coefficients are calculated using boundary and interface conditions as.

$$B_{I\theta}|_{r=R_{or}+\delta/2} = B_{II\theta}|_{r=R_{si}} \alpha_i + \frac{f}{2} < \alpha < \alpha_i - \frac{f}{2} \quad (31)$$

$$B_{I\theta}|_{r=R_{or}+\delta/2} = B_{II\theta}|_{r=R_{si}} \alpha_j + \frac{g}{2} < \alpha < \alpha_j - \frac{g}{2} \quad (32)$$

where f and g are stator slot and stator tooth opening angle respectively.

For MFD computation, since interface conditions are in the form of Fourier series with different interval it's right and left-hand side are transformed to same interval. The left and right-hand side Fourier series over interval of $[-\pi, \pi]$ is

$$\left[\alpha_i - \frac{f}{2}, \alpha_i + \frac{f}{2} \right] or \left[\alpha_j - \frac{f}{2}, \alpha_j + \frac{f}{2} \right] \quad (33)$$

GVP over boundary condition by expending Fourier series in interval of $[-\pi, \pi]$ can be expressed as

$$A_{I\theta}|_{r=R_{or}+\delta/2} = A_{II\theta}|_{r=R_{si}} \alpha_i + \frac{f}{2} < \alpha < \alpha_i - \frac{f}{2} \quad (34)$$

$$A_{I\theta}|_{r=R_{or}+\delta/2} = A_{II\theta}|_{r=R_{si}} \alpha_j + \frac{g}{2} < \alpha < \alpha_j - \frac{g}{2} \quad (35)$$

Boundary and interface conditions become feasible when left and right-hand side Fourier series over interval become

$$\left[\alpha_i - \frac{f}{2}, \alpha_i + \frac{f}{2} \right] or \left[\alpha_j - \frac{g}{2}, \alpha_j + \frac{g}{2} \right] \quad (36)$$

Utilizing the above-mentioned boundary and interface conditions, Fourier coefficient are related as follow

$$C_i \left(\frac{R_{si}}{R_{si}} \right)^{\frac{m\pi}{f}} + D_i = \sum_k \left[\left(A_{IIk} + B_{IIk} \left(\frac{R_{ri}}{R_{si}} \right)^k \right) \frac{2\pi\eta_{si}}{f} + \left(C_{IIk} + D_{IIk} \left(\frac{R_{ri}}{R_{si}} \right)^k \right) \frac{2\pi\varepsilon_{si}}{g} \right] \quad (37)$$

$$C_j \left(\left(\frac{R_{si}}{R_{PM}} \right)^{2\frac{l\pi}{g}} + 1 \right) = \sum \left[\left(A_{IIk} + B_{IIk} \left(\frac{R_{ri}}{R_{si}} \right)^k \right) \frac{2\pi\eta_{si}}{f} + \left(C_{IIk} + D_{IIk} \left(\frac{R_{ri}}{R_{si}} \right)^k \right) \frac{2\pi\varepsilon_{si}}{g} \right] \quad (38)$$

E. FOURIER COEFFICIENT

In rotor yoke B_θ of MFD component is zero, the boundary condition for B_θ becomes as

$$B_{I\theta}|_{r=h_{si}} = -\frac{1}{\mu_r} M_\theta = 0 \quad (39)$$

Utilizing boundary condition i.e. $M_\theta = 0$, B_r MFD component as follow

$$\sum_k \left[\frac{A_{Ik}}{R_{ri}} \left(\frac{R_{ri}}{R_{ri}} \right)^{k-1} - \frac{B_{Ik}}{R_{ri}} \left(\frac{R_{ri}}{R_{si}} \right)^{-k-1} + \frac{\mu_o M_{ck}}{(k^2-1)} \right] \cos(k\alpha) \sum_k \left[\frac{C_{Ik}}{R_{ri}} \left(\frac{R_{ri}}{R_{ri}} \right)^{k-1} - \frac{D_{Ik}}{R_{ri}} \left(\frac{R_{ri}}{R_{si}} \right)^{-k-1} + \frac{\mu_o M_{sk}}{(k^2-1)} \right] \sin(k\alpha) = 0 \quad (40)$$

$$\frac{A_{Ik}}{R_{ri}} \left(\frac{R_{ri}}{R_{ri}} \right)^{k-1} - \frac{B_{Ik}}{R_{ri}} \left(\frac{R_{ri}}{R_{si}} \right)^{-k-1} + \frac{\mu_o M_{ck}}{(k^2-1)} = 0 \quad (41)$$

$$\frac{C_{Ik}}{R_{ri}} \left(\frac{R_{ri}}{R_{ri}} \right)^{k-1} - \frac{D_{Ik}}{R_{ri}} \left(\frac{R_{ri}}{R_{si}} \right)^{-k-1} + \frac{\mu_o M_{sk}}{(k^2-1)} = 0 \quad (42)$$

Solving for unknown Fourier coefficient i.e. B_{Ik} and D_{Ik} in term of A_{Ik} and C_{Ik} are expressed as

$$B_{Ik} = \frac{A_{Ik} \left(\frac{R_{ri}}{R_{si}} \right)^k + \mu_o R_{ri} (k M_{\theta ck} - M_{rsk})}{(k^2-1)} \quad (43)$$

$$D_{Ik} = \frac{C_{Ik} \left(\frac{R_{ri}}{R_{si}} \right)^k + \mu_o R_{ri} (k M_{\theta ck} + M_{rsk})}{(k^2-1)} \quad (44)$$

The vector potential becomes as

$$A_{ZI} = \sum_k (K_{Ik} A_{Ik} + K_{2k} M_{\theta ck} - K_{3k} M_{rsk}) \cos(k\alpha) + \sum_k (K_{Ik} C_{Ik} + K_{2k} M_{\theta sk} + K_{3k} M_{rck}) \sin(k\alpha) \quad (45)$$

where as

$$K_{Ik} = \left[\left(\frac{r}{R_{ri}} \right)^k + \left(\frac{R_{ri}}{R_{si}} \right)^k \left(\frac{r}{R_{ri}} \right)^{-k} \right] \quad (46)$$

$$K_{2k} = \frac{\mu_o}{(k^2-1)} \left[R_{ri} k \left(\frac{r}{R_{ri}} \right)^{-k} + r \right] \quad (47)$$

$$K_{3k} = \frac{\mu_o}{(k^2-1)} \left[R_{ri} \left(\frac{r}{R_{ri}} \right)^{-k} + kr \right] \quad (48)$$

The interface condition on magnet becomes as follow due to continuity of flux density.

$$B_{Ir}|_{r=R_{PM}} = B_{IIr}|_{r=R_{PM}} \quad (49)$$

$$K_{Ik} A_{Ik} + K_{2k} M_{\theta ck} - K_{3k} M_{rsk}|_{r=R_{PM}} = A_{IIk} \left(\frac{R_{ri}}{R_{si}} \right)^k + B_{IIk} \quad (50)$$

$$K_{Ik}A_{Ik} + K_{2k}M_{\theta ck} - K_{3k}M_{rck}|_{r=R_{PM}} = C_{IIk}\left(\frac{R_{ri}}{R_{si}}\right)^{k} + D_{IIk} \tag{51}$$

$$A_{Ik}\left(1+\left(\frac{R_{ri}}{R_{si}}\right)^{2k}\right)+\frac{\mu_o}{(k^2-1)}\left[\left(R_{ri}k\left(\frac{R_{ri}}{R_{si}}\right)^{k}+R_{ri}\right)M_{\theta ck} - \left(R_{ri}\left(\frac{R_{ri}}{R_{si}}\right)^{k}+kR_{ri}\right)M_{rsk}\right] = A_{IIk}\left(\frac{R_{ri}}{R_{si}}\right)^{k}+B_{IIk} \tag{52}$$

$$C_{Ik}\left(1+\left(\frac{R_{ri}}{R_{si}}\right)^{2k}\right)+\frac{\mu_o}{(k^2-1)}\left[\left(R_{ri}k\left(\frac{R_{ri}}{R_{si}}\right)^{k}+R_{ri}\right)M_{\theta ck} - \left(R_{ri}\left(\frac{R_{ri}}{R_{si}}\right)^{k}+kR_{ri}\right)M_{rck} = C_{IIk}\left(\frac{R_{ri}}{R_{si}}\right)^{k}+D_{IIk} \tag{53}$$

$$A_{Ik}\left(1-\left(\frac{R_{ri}}{R_{si}}\right)^{2k}\right)+\frac{\mu_o}{(k^2-1)}\left[k\left(R_{ri}-R_{ri}\left(\frac{R_{ri}}{R_{si}}\right)^{k}\right)M_{\theta ck} - \left(R_{ri}-R_{ri}\left(\frac{R_{ri}}{R_{si}}\right)^{k}\right)M_{rsk} = \mu_r A_{IIk}S_4 - B_{IIk} \tag{54}$$

$$C_{Ik}\left(1-\left(\frac{R_{ri}}{R_{si}}\right)^{2k}\right)+\frac{\mu_o}{(k^2-1)}\left[k\left(R_{ri}-R_{ri}\left(\frac{R_{ri}}{R_{si}}\right)^{k}\right)M_{\theta ck} - \left(R_{ri}-R_{ri}\left(\frac{R_{ri}}{R_{si}}\right)^{k}\right)M_{rck} = \mu_r C_{IIk}\left(\frac{R_{ri}}{R_{si}}\right)^{k}+D_{IIk} \tag{55}$$

Since our primal interest is the MFD components in the mid of air gap under no-load and on-load conditions therefor, set of first order multivariable equations are solved for Harmonics coefficients calculation in the following section.

F. FOURIER COEFFICIENT CALCULATION

Employing boundary condition of infinite permeability of rotor yoke and continues scalar potential of B_r and B_θ MFD components at $r = R_{or} + \delta/2$, the harmonic coefficient in the mid of the air gap for B_r and B_θ MFD components can be derived as

$$A_{Ik} = \frac{(k_{Brc}+k_{B\theta s})}{-\mu_o k}\frac{R_{ri}^{k+1}}{R_{si}^{2k}} + B_{1k}A_{2k}\sum_i\sum_m C_i(m)X_m\eta_{si}(m,k) \tag{56}$$

$$B_{Ik} = \frac{(k_{Brc}+k_{B\theta s})}{\mu_o k}R_{ri}^{k+1} - B_{2k}A_{3k}\sum_i\sum_m C_i(m)X_m\eta_{si}(m,k) \tag{57}$$

$$C_{Ik} = \frac{(k_{Brs}-k_{B\theta c})}{-\mu_o k}\frac{R_{ri}^{k+1}}{R_{si}^{2k}} + B_{2k}A_{2k}\sum_i\sum_m C_i(m)X_m\varepsilon_{si}(m,k) \tag{58}$$

$$D_{Ik} = \frac{(k_{Brs}-k_{B\theta c})}{\mu_o k}R_{ri}^{k+1} + B_{2k}A_{3k}\sum_i\sum_m C_i(m)X_m\varepsilon_{si}(m,k) \tag{59}$$

where

$$\eta_{si} = s\eta_s(\mathrm{m},\mathrm{k})\cos(\alpha_i k) - \varepsilon_s(\mathrm{m},\mathrm{k})\sin(\alpha_i k) \tag{60}$$

$$\varepsilon_{si} = \eta_s(\mathrm{m},\mathrm{k})\sin(\alpha_i k) + \varepsilon_s(\mathrm{m},\mathrm{k})\cos(\alpha_i k) \tag{61}$$

$$[0.2pc]\eta_s(\mathrm{m},\mathrm{k}) = \begin{cases} \dfrac{2mb_{ao}\cos(0.5kb_{ao})\sin^2(0.5m\pi)}{m^2\pi^2-k^2b_{ao}^2}, & m\pi \neq kb_{ao} \\ 0.5b_{ao}\sin(0.5m\pi), & m\pi = kb_{ao} \end{cases} \tag{62}$$

$$\varepsilon_s(\mathrm{m},\mathrm{k}) = \begin{cases} \dfrac{-2mb_{ao}\sin(0.5kb_{ao})\cos^2(0.5m\pi)}{m^2\pi^2-k^2b_{ao}^2}, & m\pi \neq kb_{ao} \\ 0.5b_{ao}\cos(0.5m\pi), & m\pi = kb_{ao} \end{cases} \tag{63}$$

$$k_{Brc} = A_{1k}\gamma(k)M_{rck} \tag{64}$$

$$k_{Brs} = A_{1k}\gamma(k)M_{rsk} \tag{65}$$

$$k_{B\theta s} = A_{1k}\zeta(k)M_{rsk} \tag{66}$$

$$k_{B\theta c} = A_{1k}\zeta(k)M_{rck} \tag{67}$$

For inner rotor SPMSFCPM

$$\rho = (\mu_r+1)\left[1-\left(\frac{R_{ri}}{R_{si}}\right)^{2k}\right]-(\mu_r+1)\left[\left(\frac{R_{ri}}{R_{si}}\right)^{2k}-\left(\frac{R_{or}}{R_{ri}}\right)^{2k}\right] \tag{68}$$

$$\gamma = \frac{2}{\rho(k^2-1)}\left[(1-k)-2\left(\frac{R_{or}}{R_{ri}}\right)^{k+1}+(k+1)\left(\frac{R_{or}}{R_{ri}}\right)^{2k}\right] \tag{69}$$

$$\zeta = \frac{2}{\rho(k^2-1)}\left[(1-k)-2k\left(\frac{R_{or}}{R_{ri}}\right)^{k+1}+(k+1)\left(\frac{R_{or}}{R_{ri}}\right)^{2k}\right] \tag{70}$$

$$A_{1k} = -0.5k\mu_o \tag{71}$$

$$A_{2k} = \frac{1}{\rho}\left[(\mu_r+1)+(\mu_r-1)\left(\frac{R_{or}}{R_{ri}}\right)^{2k}\right] \tag{72}$$

$$A_{3k} = \frac{1}{\rho}\left[(\mu_r-1)+(\mu_r+1)\left(\frac{R_{or}}{R_{ri}}\right)^{2k}\right] \tag{73}$$

$$B_{1k} = R_{si}^{-k} \tag{74}$$

$$B_{2k} = R_{si}^{-k}R_{ri}^{2k} \tag{75}$$

$$X_m = \left(\frac{R_{si}}{R_{sy}}\right)^{\frac{m\pi}{b_o a}} - \left(\frac{R_{si}}{R_{sy}}\right)^{-\frac{m\pi}{b_o a}} \tag{76}$$

$$b_o a = \frac{b_o}{R_{si}} \tag{77}$$

For outer rotor SPMSFCPM

$$\rho = (\mu_r+1)\left[\left(\frac{R_{si}}{R_{ri}}\right)^{2k}-1\right]-(\mu_r+1)\left[\left(\frac{R_{ri}}{R_{si}}\right)^{2k}-\left(\frac{R_{si}}{R_{ri}}\right)^{2k}\right] \tag{78}$$

$$\gamma = \frac{2}{\rho(k^2-1)}\left[(1-k)\left(\frac{R_{ri}}{R_{ro}}\right)^{2k}-2\left(\frac{R_{ri}}{R_{or}}\right)^{k-1}+(k+1)\right] \tag{79}$$

$$\zeta = \frac{2}{\rho(k^2-1)}\left[(k-1)\left(\frac{R_{ri}}{R_{or}}\right)^{2k}-2k\left(\frac{R_{or}}{R_{ri}}\right)^{k-1}+(k+1)\right] \tag{80}$$

$$A_{1k} = -0.5k\mu_o \tag{81}$$

$$A_{2k} = \frac{1}{\rho}\left[(\mu_r+1)\left(\frac{R_{ri}}{R_{or}}\right)^{2k} + (\mu_r-1)\right] \tag{82}$$

$$A_{3k} = \frac{1}{\rho}\left[(\mu_r-1)\left(\frac{R_{ri}}{R_{or}}\right)^{2k} + (\mu_r+1)\right] \tag{83}$$

$$B_{1k} = R_{si}^{k} R_{ri}^{-2k} \tag{84}$$

$$B_{2k} = R_{si}^{k} \tag{85}$$

Now the problem left only for calculation of $C_i(m)$ of ϕ_{Ii}, the boundary condition is applied such that B_r MFD at stator opening should be continuous.

$$B_{IIIir}| = -\mu_o \sum_m \delta_m C_i(m) * sin\left[\frac{m\pi}{b_o a}\left(\alpha + \frac{b_o a}{2} - \alpha_i\right)\right] \tag{86}$$

$$\delta_m = \frac{R_{ri}}{R_{sy}}\left[\left(\left(\frac{R_{si}}{R_{sy}}\right)^{\frac{m\pi}{b_o a}-1}\right) + \left(\frac{R_{si}}{R_{sy}}\right)^{-\frac{m\pi}{b_o a}-1}\right] \tag{87}$$

B_r MFD component becomes as,

$$B_{IIr}|_{r=R_{or}+\frac{\sigma}{2}} = -\mu_o \sum_k k\left[\left(A_{II}(k) R_{si}^{k-1} - B_{II}(k) R_{si}^{-k-1}\right)\right] \cos(\alpha k) - \mu_o \sum_k k\left[\left(C_{II}(k) R_{si}^{k-1} - D_{II}(k) R_{si}^{-k-1}\right)\right] \sin(\alpha k) \tag{88}$$

Thus

$$B_{IIIir}|_{r=R_{si}} = B_{IIr}|_{r=R_{PM}} \tag{89}$$

$$\alpha_i - \frac{b_o a}{2} \le \alpha \le \alpha_i + \frac{b_o a}{2} \tag{90}$$

$B_{iir}|_{r=R_{PM}}$ is expanded into Fourier series over the i_{th} slot opening.

$$B_{IIr}|_{r=R_{PM}} = -\mu_o \sum_m C_i(m) sin\left[\frac{m\pi}{b_o a}\left(\alpha + \frac{b_o a}{2} - \alpha_i\right)\right] \tag{91}$$

$$\alpha_i - \frac{b_o a}{2} \le \alpha \le \alpha_i + \frac{b_o a}{2} \tag{92}$$

$$\delta_m C_i(m) = \sum_k k\left[(G_1(k)\,\delta_{si}(m,k) + G_2(k)\,\mathrm{T}_{si}(m,k))\right] - \sum_k k\lambda(k)\,\delta_{si}(m,k)\sum_l\sum_j C_l(j) X_j \eta_{sl}(j,k) - \sum_k k\lambda(k)\,\mathrm{T}_{si}(m,k)\sum_l\sum_j C_l(j) X_j \varepsilon_{sl}(j,k) \tag{93}$$

$$\delta_m C_i(m) = \sum_k k\left[\left(A_{II}(k) R_{si}^{k-1} - B_{II}(k) R_{si}^{-k-1}\right)\right]\delta_{si}(m,k) + k\left[\left(C_{II}(k) R_{si}^{k-1} - D_{II}(k) R_{si}^{-k-1}\right)\right]\mathrm{T}_{si}(m,k) \tag{94}$$

$$C_i(m) = \sum_k k\left[\left(A_{II}(k) R_{si}^{k-1} - B_{II}(k) R_{si}^{-k-1}\right)\right]\delta_{si}(m,k) + k\left[\left(C_{II}(k) R_{si}^{k-1} - D_{II}(k) R_{si}^{-k-1}\right)\right]\mathrm{T}_{si}(m,k) \tag{95}$$

whereas

$$\delta_{si}(m,k) = \frac{2\pi}{b_o a}\eta_{si}(m,k) \tag{96}$$

$$\mathrm{T}_{si}(m,k) = \frac{2\pi}{b_o a}\varepsilon_{si}(m,k) \tag{97}$$

$$A_{II} R_{si}^{k-1} - B_{II} R_{si}^{-k-1} = G_1 - \lambda \sum_i \sum_m C_i(m) X_m \eta_{si}(m,k) \tag{98}$$

$$C_{II} R_{si}^{k-1} - D_{II} R_{si}^{-k-1} = G_2 - \lambda \sum_i \sum_m C_i(m) X_m \varepsilon_{si}(m,k) \tag{99}$$

whereas G_1, G_2 and λ varies for inner and outer rotor topologies.

For inner rotor SPMSFCPM topologies

$$G_1 = \left(\frac{R_{ri}}{R_{si}}\right)^{k+1}\left[\gamma(k) M_{rck} + \zeta(k) M_{\theta sk}\right] \tag{100}$$

$$G_2 = \left(\frac{R_{ri}}{R_{si}}\right)^{k+1}\left[\gamma(k) M_{rsk} - \zeta(k) M_{\theta sk}\right] \tag{101}$$

$$\lambda = -R_{si}^{-1}\left[A_{2k} + A_{3k}\left(\frac{R_{ri}}{R_{si}}\right)^{2k}\right] \tag{102}$$

For outer rotor SPMSFCPM topologies

$$G_1 = \left(\frac{R_{si}}{R_{ri}}\right)^{k-1}\left[\gamma(k) M_{rck} + \zeta(k) M_{\theta sk}\right] \tag{103}$$

$$G_2 = \left(\frac{R_{si}}{R_{ri}}\right)^{k-1}\left[\gamma(k) M_{rsk} - \zeta(k) M_{\theta sk}\right] \tag{104}$$

$$\lambda = -R_{si}^{-1}\left[A_{2k}\left(\frac{R_{si}}{R_{ri}}\right)^{2k} + A_{3k}\right] \tag{105}$$

G. ROTOR POLE AND SLOT COMBINATION

Various rotor pole and slot combination for design of SPMSFCPM exist. The feasible rotor poles and stator slots combination of the proposed model is calculated utilizing equation (107) and equation (108) as follow [28].

$$N_s = km \tag{106}$$

$$N_r = 2Z_s \pm k \tag{107}$$

whereas m represent phases number, k is integer, N_s and N_r are stator slot and rotor pole number, respectively.

Based on electromagnetic performance for wide range rotor pole number, rotor pole number 13 offer better electromagnetic performance and considered for detailed investigation.

IV. COMPUTATION OF ELECTROMAGNETIC PERFORMANCE

The electromagnetic performance including B_r and B_θ MFD components under no-load and on-load condition, Open

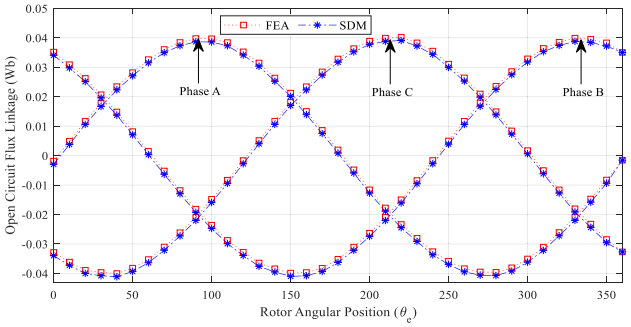

FIGURE 6. Prediction of Φ by FEA and SDM.

Circuit Flux linkage (Φ), cogging torque (T_{cog}) and instantaneous torque (T_{ins}) are considered as key matric function for validation of analytical SDM for design of SPMSFCPM. Electromagnetic performance is computed based on GVP and Maxwell Stress Tensor utilizing MFD components.

Φ for one phase is the summation of flux linkage linked with all coil sets of the phase. GVP based computation of Φ is expressed as [26]

$$\Phi = \frac{LN}{A}\int_{R_{si}}^{R_{sy}}\int_{\alpha_1}^{\alpha_2} A_z \, rdrd\alpha \tag{108}$$

$$\Phi = \frac{LN}{A}\int_{R_{si}}^{R_{sy}}\int_{\alpha_1}^{\alpha_2+0.5d_{sa}} A_z \, rdrd\alpha \tag{109}$$

T_{cog} is calculated based on sine and cosine B_r and B_θ components of MFD utilizing Maxwell Stress Tensor (MST) method [7], [27]

$$T_{cog} = \frac{r^2L}{\mu_o}\int_0^{2\pi} B_{Ir}B_{I\theta}d\theta = \frac{\pi r^2L}{\mu_o}\sum_k B_{rck}B_{\theta ck} + B_{rsk}B_{\theta sk} \tag{110}$$

whereas B_{rsk} and B_{rck} are radial sine and cosine MFD components respectively, $B_{\theta sk}$ and $B_{\theta ck}$ are tangential sine and cosine MFD components respectively.

Furthermore, T_{ins} is calculated based on B_r and B_θ components in the mid of air-gap using MST method [1], [3]

$$T_{ins} = \frac{r^2L}{\mu_o}\int_0^{2\pi} B_{Ir}B_{I\theta}d\theta \tag{111}$$

V. VALIDATION OF ANALYTICAL SUB-DOMAIN MODELLING FOR INITIAL DESIGN OF SPMSFCPM

The developed SDM is validated with globally accepted FEA based on SPMSFCPM design parameters shown in table 1. To obtained accurate and precise electromagnetic performance, 2D Transient magnetic field analysis is carried out with rated armature current density of 15 A/mm^2 and rotational speed of 1200 RPM. Note that FEA is performed utilizing JMAG Commercial FEA Package v. 18.1.

Open circuit flux linkage of developed SPMSFCPM predicted by SDM and FEA are shown in Figure 6. Analysis discloses that open circuit flux linkage predicted by SDM and FEA confirm decent agreement with absolute ultimate error of $\sim 1\%$.

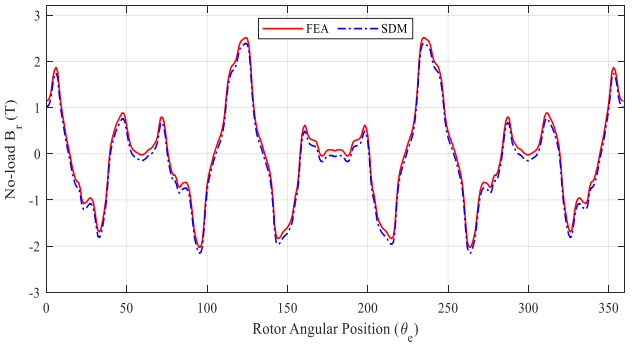

FIGURE 7. Prediction of no-load B_r using SDM and FEA.

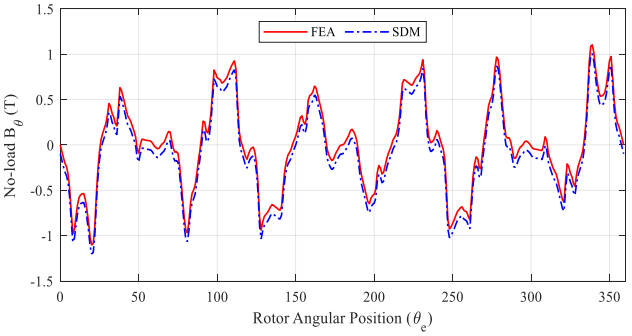

FIGURE 8. Prediction of no-load B_θ using SDM and FEA.

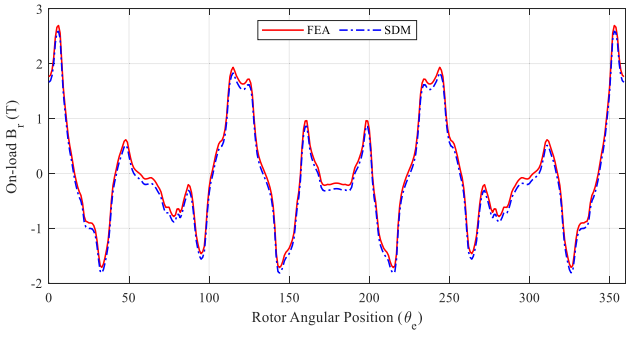

FIGURE 9. Prediction of on-load B_r using SDM and FEA.

Moreover, no-load and on-load MFD components i.e. B_r and B_θ in design of SPMSFCPM in the mid of air-gap utilizing SDM is calculated. No load B_r and B_θ calculated by FEA and SDM are shown in Figure 7 and Figure 8 respectively whereas on-load B_r and B_θ are shown in Figure 9 and Figure 10 respectively. Analysis unveil that magnetic field computation using SDM resemble FEA showing absolute peak error of $\sim 1.5\%$.

Based on B_r and B_θ sine and cosine components, T_{cog} is calculated as shown in Figure 11. It can be clearly seen that predicted SDM and FEA results exhibit good agreements with relative error of $\sim 1.98\%$.

Finally, based on on-load B_r and B_θ components of MFD, T_{ins} of initial design of SPMSFCPM is calculated as shown in Figure 12. It can be clearly seen that SDM based calculated

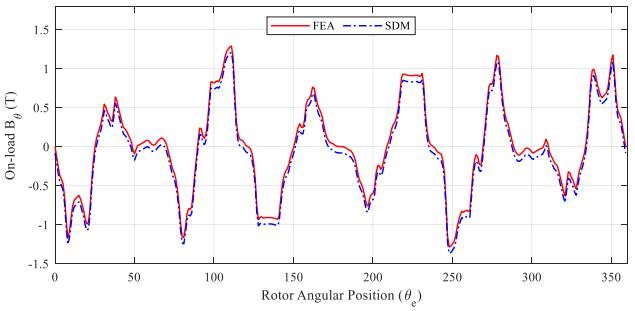

FIGURE 10. Prediction of no-load B_θ using SDM and FEA.

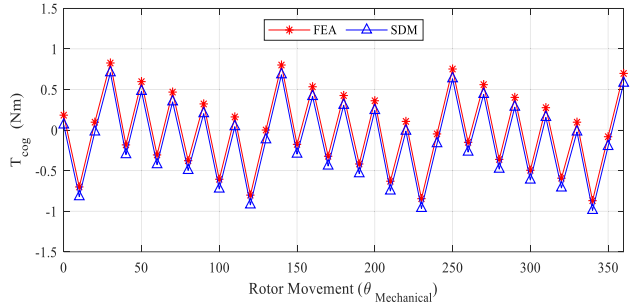

FIGURE 11. T_{cog} predicted by FEA and SDM.

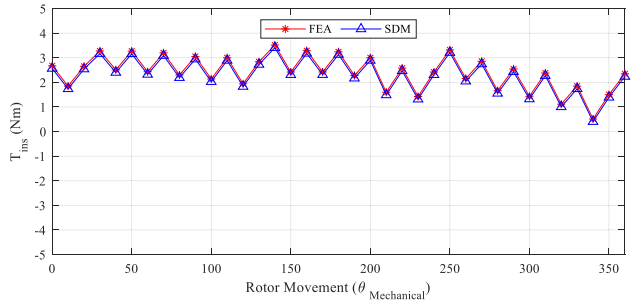

FIGURE 12. T_{ins} predicted by FEA and SDM.

T_{ins} fairly match with FEA showing maximum peak error of $\sim 1.76\%$.

VI. CONCLUSION

In this article analytical sub-domain model for magnetic field computation in SPMSFCPM is developed. Overall field domain is divided in sub-regions such as air-gap, PMs and stator slot where expressions are derived are simply utilizing boundary and interface conditions accounting influence of CM/RM-PMs and inner/outer rotor SPMSFCPM topologies. Based on magnetic field especially B_r and B_θ components electromagnetic performance such as open-circuit flux linkage, instantaneous torque and cogging torque are computed utilizing GVP and MST respectively. Analysis reveals that prediction of analytical SDM accurately match waveform and peak values of electromagnetic performance which is validated and confirmed by existing FEA. Hence, authors are confident to recommend developed analytical SDM for initial design of machine before proceeding to numerical based FEA and fabrication.

REFERENCES

[1] W. Ullah, F. Khan, and E. Sulaiman, "Sub-domain modelling and multi-variable optimisation of partitioned PM consequent pole flux switching machines," *IET Electr. Power Appl.*, vol. 14, no. 8, pp. 1360–1369, Aug. 2020.

[2] K. T. Chau, C. C. Chan, and C. Liu, "Overview of permanent-magnet brushless drives for electric and hybrid electric vehicles," *IEEE Trans. Ind. Electron.*, vol. 55, no. 6, pp. 2246–2257, Jun. 2008.

[3] W. K. Ullah, S. Faisal, U. Erwan, U. Muhammad, K. Noman, "Analytical validation of novel consequent pole E-core stator permanent magnet flux switching machine," *IET Electr. Power Appl.*, vol. 14, no. 5, pp. 789–796, 2020.

[4] T. Lubin, S. Mezani, and A. Rezzoug, "2-D exact analytical model for surface-mounted permanent-magnet motors with semi-closed slots," *IEEE Trans. Magn.*, vol. 47, no. 2, pp. 479–492, Feb. 2011.

[5] L. J. Wu, Z. Q. Zhu, D. Staton, M. Popescu, and D. Hawkins, "Analytical prediction of electromagnetic performance of surface-mounted PM machines based on subdomain model accounting for tooth-tips," *IET Electr. Power Appl.*, vol. 5, no. 7, pp. 597–609, Aug. 2011.

[6] A. Rahideh and T. Korakianitis, "Analytical magnetic field calculation of slotted brushless permanent-magnet machines with surface inset magnets," *IEEE Trans. Magn.*, vol. 48, no. 10, pp. 2633–2649, Oct. 2012.

[7] Z. Q. Zhu, L. J. Wu, and Z. P. Xia, "An accurate subdomain model for magnetic field computation in slotted surface-mounted permanent-magnet machines," *IEEE Trans. Magn.*, vol. 46, no. 4, pp. 1100–1115, Apr. 2010.

[8] F. Dubas and C. Espanet, "Analytical solution of the magnetic field in permanent-magnet motors taking into account slotting effect: No-load vector potential and flux density calculation," *IEEE Trans. Magn.*, vol. 45, no. 5, pp. 2097–2109, May 2009.

[9] T. C. O'Connell and P. T. Krein, "The schwarz-christoffel analytical method applied to electric machine slot shape optimization," in *Proc. IEEE Int. Electr. Mach. Drives Conf.*, May 2007, pp. 341–346.

[10] D. C. J. Krop, "Integration of dual electromagnetic energy conversions: Linear actuation with integrated contactless energy transfer," Ph.D. dissertation, Dept. Elect. Eng., Eindhoven Univ. Technol., Eindhoven, The Netherlands, 2013, pp. 47–74.

[11] J. R. M. van Dam, J. J. H. Paulides, W. S. P. Robertson, M. Dhaens, and E. A. Lomonova, "Analytical surface charge method for rotated permanent magnets: Boundary element method comparison and experimental validation," *IEEE Trans. Magn.*, vol. 52, no. 7, Jul. 2016, Art. no. 8001404.

[12] R. L. J. Sprangers, J. J. H. Paulides, B. L. J. Gysen, and E. A. Lomonova, "Magnetic saturation in semi-analytical harmonic modeling for electric machine analysis," *IEEE Trans. Magn.*, vol. 52, no. 2, Feb. 2016, Art. no. 8100410.

[13] B. L. J. Gysen, K. J. Meessen, J. J. H. Paulides, and E. A. Lomonova, "General formulation of the electromagnetic field distribution in machines and devices using Fourier analysis," *IEEE Trans. Magn.*, vol. 46, no. 1, pp. 39–52, Jan. 2010.

[14] K. J. W. Pluk, J. W. Jansen, and E. A. Lomonova, "Hybrid analytical modeling: Fourier modeling combined with mesh-based magnetic equivalent circuits," *IEEE Trans. Magn.*, vol. 51, no. 8, pp. 1–10, Aug. 2015.

[15] S. Ouagued, Y. Amara, and G. Barakat, "Comparison of hybrid analytical modelling and reluctance network modelling for pre-design purposes," *Math. Comput. Simul.*, vol. 130, pp. 3–21, Dec. 2016.

[16] S. Ouagued, A. Aden Diriye, Y. Amara, and G. Barakat, "A general framework based on a hybrid analytical model for the analysis and design of permanent magnet machines," *IEEE Trans. Magn.*, vol. 51, no. 11, pp. 1–4, Nov. 2015.

[17] S. Ouagued, Y. Amara, and G. Barakat, "Cogging force analysis of linear permanent magnet machines using a hybrid analytical model," *IEEE Trans. Magn.*, vol. 52, no. 7, Jul. 2016, Art. no. 8202704.

[18] Y. Laoubi, M. Dhifli, G. Verez, Y. Amara, and G. Barakat, "Open circuit performance analysis of a permanent magnet linear machine using a new hybrid analytical model," *IEEE Trans. Magn.*, vol. 51, no. 3, Mar. 2015, Art. no. 8102304.

[19] E. Ilhan, B. L. J. Gysen, J. J. H. Paulides, and E. A. Lomonova, "Analytical hybrid model for flux switching permanent magnet machines," *IEEE Trans. Magn.*, vol. 46, no. 6, pp. 1762–1765, Jun. 2010.

[20] N. Ullah, F. Khan, W. Ullah, A. Basit, M. Umair, and Z. Khattak, "Analytical modelling of open-circuit flux linkage, cogging torque and electromagnetic torque for design of switched flux permanent magnet machine," *J. Magn.*, vol. 23, no. 2, pp. 253–266, Jun. 2018.
[21] N. Ullah, F. Khan, W. Ullah, M. Umair, and Z. Khattak, "Magnetic equivalent circuit models using global reluctance networks methodology for design of permanent magnet flux switching machine," in *Proc. 15th Int. Bhurban Conf. Appl. Sci. Technol. (IBCAST)*, Jan. 2018, pp. 397–404.
[22] Z. Q. Zhu, Y. Pang, D. Howe, S. Iwasaki, R. Deodhar, and A. Pride, "Analysis of electromagnetic performance of flux-switching permanent-magnet machines by nonlinear adaptive lumped parameter magnetic circuit model," *IEEE Trans. Magn.*, vol. 41, no. 11, pp. 4277–4287, Nov. 2005.
[23] W. Ullah, F. Khan, and M. Umair, "Lumped parameter magnetic equivalent circuit model for design of segmented PM consequent pole flux switching machine," *Eng. Comput.*, early access, Jul. 2020, doi: 10.1108/EC-04-2020-0201.
[24] Z. Q. Zhu, D. Howe, and C. C. Chan, "Improved analytical model for predicting the magnetic field distribution in brushless permanent-magnet machines," *IEEE Trans. Magn.*, vol. 38, no. 1, pp. 229–238, Jan. 2002.
[25] L. J. Wu, Z. Q. Zhu, D. Staton, M. Popescu, and D. Hawkins, "Analytical modeling of eddy current loss in retaining sleeve of surface-mounted PM machines accounting for influence of slot opening," in *Proc. IEEE Int. Symp. Ind. Electron.*, May 2012, pp. 611–616.
[26] K. J. Binns, P. J. Lawrenson, and C. W. Trowbridge, *The Analytical and Numerical Solution of Electric and Magnetic Fields*. Hoboken, NJ, USA: Wiley, 1992.
[27] T. L. Tiang, D. Ishak, C. P. Lim, and M. K. M. Jamil, "A comprehensive analytical subdomain model and its field solutions for surface-mounted permanent magnet machines," *IEEE Trans. Magn.*, vol. 51, no. 4, Apr. 2015, Art. no. 8104314.
[28] J. T. Chen, Z. Q. Zhu, S. Iwasaki, and R. P. Deodhar, "A novel E-Core switched-flux PM brushless AC machine," *IEEE Trans. Ind. Appl.*, vol. 47, no. 3, pp. 1273–1282, May 2011.

WASIQ ULLAH was born in Peshawar, Pakistan, in 1995. He received the B.S. and M.S. degrees in electrical (power) engineering from COMSATS University Islamabad (Abbottabad Campus), Abbottabad, Pakistan, in 2018 and 2020, respectively, where he is currently pursuing the Ph.D. degree in electrical (power) engineering.

Since 2018, he has been a Research Associate with the Electric Machine Design Research Group. His research interests include analytical modeling, design analysis, and optimization of permanent magnet flux switching machines, linear flux switching machines, hybrid excited flux switching machines, and novel consequent pole flux switching machines for high-speed brushless AC applications.

FAISAL KHAN (Member, IEEE) was born in Charsada, Pakistan, in 1986. He received the B.S. degree in electronics engineering and the M.S. degree in electrical engineering from COMSATS University Islamabad, Abbottabad Campus, Pakistan, in 2009 and 2012, respectively, and the Ph.D. degree in electrical engineering from Universiti Tun Hussein Onn Malaysia, Malaysia, in 2017.

From 2010 to 2012, he was a Lecturer with the University of Engineering and Technology, Abbottabad, Pakistan. Since 2017, he has been an Assistant Professor with the Department of Electrical Engineering, COMSATS University Islamabad, Abbottabad Campus. He has authored more than 70 publications and one patent. He has received multiple research awards. His research interests include design and analysis of flux-switching machines, synchronous machines, and DC machines.

ERWAN SULAIMAN was born in Johor, Malaysia, in 1978. He received the B.E. degree in electrical engineering from the University of Malaya in 2001, the M.E. degree in electrical engineering from University Tun Hussein Onn Malaysia (UTHM) in 2004, and the Ph.D. degree in electrical engineering from the Nagoya Institute of Technology, Japan, in 2012. He has been a Lecturer with UTHM since 2004, where he is currently a Professor with the Department of Electrical Power Engineering. His research interests include design optimizations of hybrid excited flux switching machines and wound field flux switching machines for electric vehicles and hybrid electric vehicles drive applications.

IRFAN SAMI received the B.Sc. degree in electrical engineering from the University of Engineering and Technology Peshawar, Bannu Campus, Pakistan, in 2016, and the M.Sc. degree in electrical engineering from COMSATS University Islamabad, Abbottabad Campus, Abbottabad, Pakistan, in 2019. He is currently pursuing the Ph.D. degree in electrical engineering with the Chung-Ang University, Seoul, South Korea. His research interests include electric drives, renewable energies, and electrical machine design.

JONG-SUK RO received the B.S. degree in mechanical engineering from Han-Yang University, Seoul, South Korea, in 2001, and the Ph.D. degree in electrical engineering from the Seoul National University (SNU), Seoul, in 2008.

In 2014, he was with the University of Bath, Bath, U.K., as an Academic Visitor. From 2013 to 2016, he was with the Brain Korea 21 Plus, SNU, as a BK Assistant Professor. He conducted research with the Electrical Energy Conversion System Research Division, Korea Electrical Engineering and Science Research Institute, as a Researcher, in 2013. From 2012 to 2013, he was with the Brain Korea 21 Information Technology, SNU, as a Post-Doctoral Fellow. He conducted research with the Research and Development Center, Samsung Electronics, as a Senior Engineer, from 2008 to 2012. He is currently an Associate Professor with the School of Electrical and Electronics Engineering, Chung-Ang University, Seoul. His research interests include analysis and optimal design of next-generation electrical machines using smart materials, such as electromagnet, piezoelectric, and magnetic shape memory alloy.